

Tuning the Diameter, Stability, and Membrane Affinity of Peptide Pores by DNA-Programmed Self-Assembly

Aziz Fennouri,[‡] Jonathan List,[‡] Julie Ducrey, Jessica Dupasquier, Viktorija Sukyte, Simon F. Mayer, Reyner D. Vargas, Laura Pascual Fernandez, Frederick Bertani, Sandra Rodriguez Gonzalo, Jerry Yang, and Michael Mayer*



Cite This: *ACS Nano* 2021, 15, 11263–11275



Read Online

ACCESS |



Metrics & More



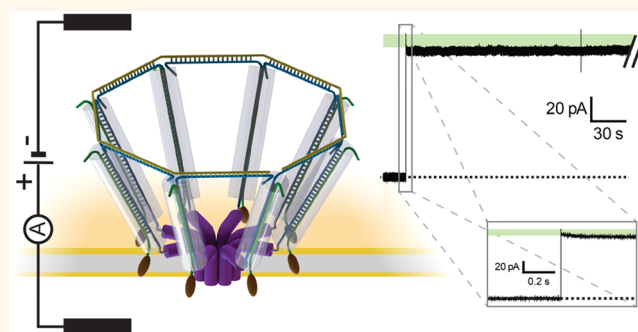
Article Recommendations



Supporting Information

ABSTRACT: Protein pores recently enabled a breakthrough in bioanalytics by making it possible to sequence individual DNA and RNA strands during their translocation through the lumen of the pore. Despite this success and the overall promise of nanopore-based single-molecule analytics, protein pores have not yet reached their full potential for the analysis and characterization of globular biomolecules such as natively folded proteins. One reason is that the diameters of available protein pores are too small for accommodating the translocation of most folded globular proteins through their lumen. The work presented here provides a step toward overcoming this limitation by programmed self-assembly of α -helical pore-forming peptides with covalently attached single-stranded DNA (ssDNA). Specifically, hybridization of the peptide ceratotoxin A (CtxA) with N-terminally attached ssDNA to a complementary DNA template strand with 4, 8, or 12 hybridization sites made it possible to trigger the assembly of pores with various diameters ranging from approximately 0.5 to 4 nm. Hybridization of additional DNA strands to these assemblies achieved extended functionality in a modular fashion without the need for modifying the amino acid sequence of the peptides. For instance, functionalization of these semisynthetic biological nanopores with DNA–cholesterol anchors increased their affinity to lipid membranes compared to pores formed by native CtxA, while charged transmembrane segments prolonged their open-state lifetime. Assembly of these hybrid DNA–peptides by a template increased their cytotoxic activity and made it possible to kill cancer cells at 20-fold lower total peptide concentrations than nontemplated CtxA.

KEYWORDS: Ceratotoxin A, pore-forming peptide, size-tunable pore, nanopore, DNA nanotechnology, programmable pore diameter



Resistive pulse sensing with nanopores makes it possible to detect, characterize, and—in the case of DNA or RNA—sequence individual molecules.^{1–5} Most of these applications use one of the following seven protein nanopores: *Mycobacterium smegmatis* porin A (MspA),^{6,7} cytolysin A (ClyA),^{8,9} bacteriophage Phi29 DNA-packaging motor,¹⁰ fragaceatoxin (FraC),^{11,12} the outer membrane lipoprotein CsgG,¹³ aerolysin,^{14–16} or α -hemolysin.^{17–19} While site-directed mutagenesis enables fine-tuning the function of these protein pores with exquisite fidelity—such as presenting amino acid side chains with desired functional groups at precisely determined locations within the nanopore lumen^{20,21}—the diameter of these pores can only be manipulated within small limits. Attempts to expand the diameter of these pores typically compromises their stability or

function,^{9,22} making it impossible to use such modified pores for the analysis of large biomolecules such as most proteins in their native state.

The emergence of DNA nanotechnology enables programmable molecular arrangement of components into complex and well-defined structures.^{23–27} In the past few years, several groups demonstrated self-assembled pores made from three-dimensional DNA origami structures. These constructs are

Received: December 9, 2020

Accepted: June 7, 2021

Published: June 15, 2021



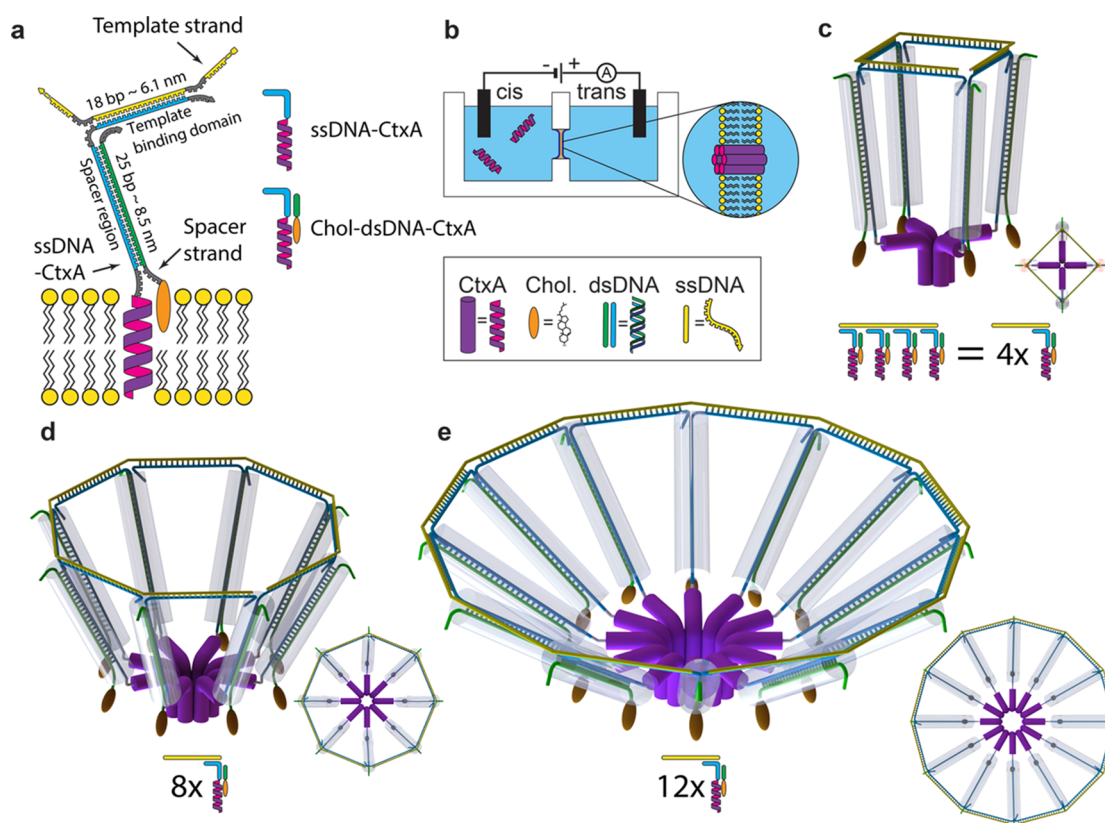


Figure 1. Schematic representation of DNA-assembled peptide pores with programmable pore size. (a) Assembly strategy mediated by DNA hybridization. The pore-forming peptide CtxA (purple) bears an N-terminally attached ssDNA (blue) with two domains: the template-binding region and the spacer region. The terminal domain binds to an ssDNA template (yellow) that presents 4, 8, or 12 complementary hybridization sites. We also conducted a limited number of experiments with a template with six hybridization sites (see [Supporting Information Section S6](#)). Hybridization of an additional DNA strand (green)—referred to as the spacer strand or the cholesterol strand when it is modified with a cholesterol moiety—adds a hydrophobic moiety (orange) that is positioned to interact with the lipid membrane and increases the membrane affinity. Four thymine nucleotides (gray) act as flexible linkers between the DNA segments. (b) Schematic representation of the planar lipid bilayer setup used to record the pore-forming activity and the single-channel conductance of CtxA pores. (c–e) Schemes, projections, and top views of idealized arrangements of template-assembled tetrameric (c), octameric (d), and dodecameric (e) CtxA–DNA pores, with fully occupied template strands containing 4, 8, or 12 binding sites for the ssDNA–CtxA monomers. CtxA peptides are represented with a kink in the α -helical secondary structure as reported by Saint et al.³⁸ Cylinders shaded in gray represent the approximate diameter of double-stranded DNA (dsDNA) relative to the diameter of CtxA. Note, the perfectly circular depictions of the DNA template with attached DNA–CtxA peptides in cartoons c–e are idealized representations. Due to several single-stranded DNA segments, these assemblies are flexible and can presumably adopt a range of conformations within their geometrical and steric constraints in solution.

often modified with hydrophobic moieties like cholesterol to stabilize these hydrophilic DNA channels in the hydrophobic core of the lipid bilayer.^{28–33} So far, these DNA pores are, however, limited by the difficulty of inserting multiple charged DNA strands into lipid bilayers, especially for large diameter pores.²⁸ In addition, pore walls made from DNA are permeable to ions, resulting in leak currents, and motion of the DNA duplexes can increase noise and induce gating of the pores.^{28,34,35}

Concurrently with our ongoing research in this area,³⁶ two research groups recently addressed these limitations by pioneering the development of hybrid pores made from pore-forming proteins or peptides attached to DNA. DNA hybridization to a template provided the assembly of these pores. This design took advantage of the insulating pore walls provided by the protein or peptide component. Specifically, Henning-Knechtel et al. suggested DNA-templated assembly of 12, 20, or 26 monomers of α -hemolysin proteins, which natively form heptameric pores.³⁷ Shortly thereafter, Hagan Bayley's group scaffolded monomers of the polysaccharide

transporter Wza, leading to exceptionally stable octameric pores in lipid bilayers, while attempts to assemble fewer than eight Wza peptides led to short-lived pores (<1 min) or to pores with the same conductivity as the octamers.²²

Here, we explored the potential of a modular DNA assembly system based on the pore-forming peptide CtxA. This 36-amino-acid peptide self-incorporates into membranes and dynamically assembles to barrel-stave pores that expand or shrink in diameter as a consequence of association or dissociation of peptide monomers similar to the pore-forming peptide alamethicin.^{38,39} CtxA peptides can form pores composed of trimers to at least decamers with diameters spanning from less than 0.5 nm to approximately 4 nm.^{38,40,41} Other advantages of CtxA, demonstrated in this work, include the formation of bilayer-spanning pores with short lengths (<6 nm), the possibility to fine-tune the diameter in well-defined, subnanometer increments, and the possibility to obtain CtxA peptides as well as all other components of the assemblies presented here from commercial sources. This latter aspect creates opportunities for broad accessibility and for reprodu-

Table 1. Comparison of the Open-State Conductance Levels of Pores from Native CtxA, Chol–dsDNA–CtxA, and Templated Chol–dsDNA–CtxA^a

open state	conductance (pS)			area-equivalent diameter (nm) ^b
	native CtxA	Chol–dsDNA–CtxA	templated Chol–dsDNA–CtxA	
O1 (3-mer)	50 ± 25	35 ± 20		<0.2
O2 (4-mer)	510 ± 30	445 ± 160	460 ± 130	0.5 ± 0.3
O3 (5-mer)	1645 ± 200	1515 ± 320		1.0 ± 0.4
O4 (6-mer)	3125 ± 305	3100 ± 170	3200 ^d	1.4 ± 0.3
O5 (7-mer)	4630	5200 ± 600		1.9 ± 0.6
O6 (8-mer)	6600	6960 ± 120	7220 ± 470	2.3 ± 0.3
O7 (9-mer)		9500 ± 400		2.8 ± 0.7
O8 (10-mer)		11 640 ^c		3.1
O9 (11-mer)		14 140 ^c		3.6
O10 (12-mer)		16 760 ^c	16 880 ± 970 ^c	4.0

^aConductance values were measured at an applied potential difference of +180 mV. ^bWe estimated the diameter from single-channel conductance values of pores composed of Chol–dsDNA–CtxA assuming a pore length of 3.5 nm and a cylindrical lumen within the lipid bilayer. Errors were calculated from standard deviation of the mean. See [Supporting Information Section 3](#) for details. ^cWe extrapolated these values from a fit to the experimental conductance data from O1 to O7 assuming a geometrical arrangement of cylindrical peptide monomers to a cylindrical barrel-stave pore (see [Supporting Information Section 3](#) for details). ^dDue to the small number of experiments that we conducted with the 6-mer template, we cannot give a meaningful error for this value. See [Supporting Information Section 6](#) for details. ^eThis conductance value was measured in 3 M CsCl in 30% (v/v) glycerol in water and converted to the corresponding value in 1 M NaCl (see [Supporting Information Section 3](#)). We used 3 M CsCl in 30% (v/v) glycerol in water with 10 mM HEPES, pH 7.4, as the buffered electrolyte for all experiments with 12-mer CtxA pores, as this solution improved the stability of the lipid membrane.

cible production—a favorable aspect if hybrid biological nanopores are to find widespread applications in bioanalytics, drug delivery, or therapeutics.⁴ Finally, native CtxA bears six positively charged amino acid side chains and thus binds stronger to the negatively charged outer membranes of many pathogen and cancer cells than to plasma membranes of typical mammalian cells, whose outer leaflet is less negatively charged at neutral pH.^{42,43}

In summary, this work presents the formation of pores, which, in comparison to pores from native CtxA, benefit from programmable diameters, increased open-state lifetimes, increased stability, and increased affinity to lipid membranes. The design based on site-specific DNA hybridization is modular, and the aforementioned desired modifications or functionalities can be implemented individually or in combination. We propose that this approach makes DNA–peptide pores attractive for detection and characterization of large biomolecules as well as for enhanced killing of cancer cells compared to native, untemplated CtxA peptides.

RESULTS AND DISCUSSION

Design Strategy for DNA-Templated Assembly of Pores from the Pore-Forming Peptide CtxA. As shown in [Figure 1](#), we designed hybrid molecules from CtxA and an ssDNA oligonucleotide with 55 nucleobases that we attached with its 5' end to the N-terminus of CtxA (ssDNA–CtxA). This ssDNA sequence consists of two parts: a 25-nucleotide-long spacer region—spanning a length of approximately 8.5 nm when extended—to accommodate geometric constraints of the assembly and an 18-nucleotide-long template-binding domain—with an extended length of approximately 6.1 nm—to promote assembly with a template strand that contains a programmable number of complementary hybridization sites. To favor the assembly of tetrameric, octameric, or dodecameric CtxA pores, we used template strands with 4, 8, or 12 hybridization sites that were each 18 nucleotides long. We show in addition, in [Supplementary Section S6](#), preliminary results of experiments conducted with hexameric

CtxA pores. Flexible linkers consisting of four thymine nucleotides connect all domains of the construct and provide flexibility to adjust to geometric constraints. [Figure 1c–e](#) illustrates the open modular design of the DNA-assembled peptide pores. Ions can flow between the strands of the DNA scaffold with the advantage that the scaffold does not significantly increase the access resistance to the pore ([Table 1](#)). Focusing the voltage drop to the pore region improves the signal-to-noise ratio for potential resistive pulse applications.⁴⁴ As shown in [Figure 1a](#), we hybridized a strand (referred to as the spacer strand) to the spacer region of ssDNA–CtxA in order to increase the rigidity of the assembly by double-strand formation. Further modification of the resulting dsDNA–CtxA peptide made it possible to incorporate additional functional groups. For example, we attached a cholesterol moiety to the 3' end of this spacer strand (Chol–dsDNA–CtxA), resulting in the functionalization of each peptide with a hydrophobic moiety that increased the affinity of the assemblies to the lipid membrane ([Figure 2](#)). We are referring to this DNA spacer strand henceforth as the cholesterol strand. [Supplementary Table S9](#) provides details about the sequences we used in this work.

Hydrophobic Functionalization Favored Pore Formation at Low Concentrations of CtxA–DNA Assemblies. To investigate the effect of cholesterol moieties, we compared single-channel recordings of pore formation by Chol–dsDNA–CtxA in the absence of a template strand with various CtxA peptides that did not contain the cholesterol group. As shown in [Figure 2](#), we kept the total concentration of all peptides constant at 5 nM for this comparison. Typically, native CtxA, ssDNA–CtxA, and dsDNA–CtxA exhibited no or infrequent pore formation at this low peptide concentration ([Figure 2a–c](#)). In contrast, a 5 nM concentration of the peptide with the cholesterol modification (Chol–dsDNA–CtxA) showed frequent pore formation ([Figure 2d](#)). These results indicate that positioning a hydrophobic group toward the lipid membrane by hybridizing an ssDNA with a terminal cholesterol moiety to the ssDNA–peptide hybrid favors its

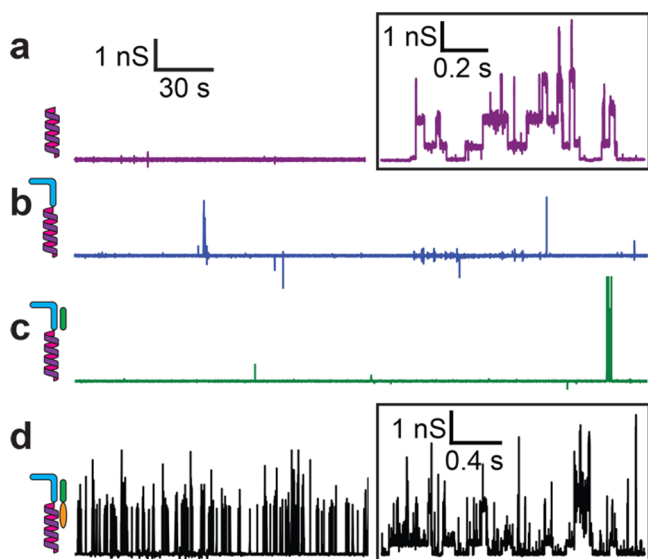


Figure 2. Effect of cholesterol on the pore-forming activity of various CtxA peptides. (a) Planar lipid bilayer recording in the presence of 5 nM peptide concentration with native CtxA. The inset of panel (a) shows typical stepwise current fluctuations from native CtxA at a peptide concentration of 20 nM. (b) Recordings in the presence of 5 nM ssDNA–CtxA or (c) 5 nM dsDNA–CtxA without a terminal cholesterol moiety; in both cases, pore formation was either absent or infrequent. (d) Experiments with 5 nM Chol–dsDNA–CtxA, which carried a cholesterol strand. The current trace in the inset shows the ability of Chol–dsDNA–CtxA to form pores with well-defined conductance levels, similar to native CtxA peptides. All recordings were performed at an applied potential difference of +180 mV.

insertion in lipid membranes. While a minimum concentration of 10 to 20 nM was necessary for native CtxA to display frequent pore formation (Figure 2a, inset), concentrations as low as 1 nM were sufficient to observe frequent pore formation by nontemplated Chol–dsDNA–CtxA peptides. After adding a template strand to the same Chol–dsDNA–CtxA molecules, we observed pore formation at concentrations as low as 0.1 nM (see Supplementary Figure S14).

Single-channel recordings of pore formation from Chol–dsDNA–CtxA, in the absence of a template strand, revealed the presence of multiple open states, like native CtxA.^{38,40,41} We report in Table 1 the single-channel conductance values of DNA-modified CtxA pores and show that they were similar to the conductance of native CtxA pores with the same number of monomers (paired-sample *t*-test revealed no statistically significant differences). We later used these values to assess the size of templated CtxA pores. The inset in Figure 2d and Figure 3a additionally show that N-terminally modified peptides retained their ability to assemble to pores with well-defined conductance states whose fluctuations were consistent with a barrel-stave model of pore formation.^{39,45,46} This result demonstrates that DNA-modified peptides were intrinsically able to adopt assemblies with a range of pore diameters, which is a critical prerequisite for assemblies to pores with programmable diameters. A comparison of conductance values in Table 1 reveals that the presence of dsDNA on the N-terminus of CtxA neither significantly changed the access resistance to the pore nor the diameter of the resulting pore assemblies.

Conventionally, pore-forming peptides are engineered by modifying the amino acid sequence of peptides to increase their pore-forming activity at low concentrations.^{47–49} The results shown in Figure 2 demonstrate that the addition of DNA strands with adequately positioned hydrophobic cholesterol moieties achieved the same effect without the need for sequence alterations. This strategy enables straightforward comparison of various moieties attached to the spacer strand (Figure 1a) to increase membrane affinity while circumventing possible undesired effects from sequence alterations such as changes in helicity, reduced membrane partitioning, or reduced propensity to assemble to pores. Moreover, the strategy presented here is modular, since it is straightforward to replace the cholesterol moiety by other desirable functional groups after attaching it to complementary ssDNA.

Addition of a DNA Template Favored the Desired Pore Size. In order to explore the concept of assembling ssDNA–CtxA peptides to nanopores with programmable diameters, we introduced a DNA template strand consisting of 4, 8, or 12 binding sites. Figure 3b shows that the relative frequency for observing different conductance levels changed drastically after addition of a 4-mer template: at the time resolution of the recording electronics, we observed predominantly conductance changes in single steps to a level that corresponded to the tetrameric pore, as expected (Figure 3b, area shaded in pink, these results are based on $N = 10$ individual experiments). The current fluctuated, however, frequently between the O1 level of a trimeric pore and the O2 level of a tetrameric pore. We hypothesize that these fluctuations resulted from reversible transitions of individual Chol–dsDNA–CtxA monomers in the templated tetrameric assembly from a membrane-spanning conformation that participated in pore formation to another conformation that did not participate in pore formation. The observed rapid switching between conductance levels of the trimeric and tetrameric pore over long recording times is consistent with a templated assembly of four CtxA monomers. Figure 3b shows that CtxA monomers that were hybridized to a DNA template could not escape the assembly, since we observed well-defined, apparent two-state open-pore switching over long recording times; escape of one CtxA molecule from the assembly would have resulted in switching between no pore and a trimeric pore with much smaller single-channel conductance (Table 1). Finally, the recorded conductance rarely exceeded the conductance level of the tetrameric pore over long recording times, further indicating that this pore comprised four monomers that were linked together; in contrast, assemblies of free CtxA monomers led to dynamic fluctuations of several different conductance levels that often exceeded the level of the tetrameric pore as shown in Figure 3a.

Increasing the number of hybridization sites on the ssDNA template resulted in the formation of pores with large transitions that frequently jumped multiple conductance levels in a period of time below the time resolution of the recordings. In the presence of an 8-mer template, we observed conductance values that were closest to the conductance of the octameric pore (Figure 3c and Table 1, $N > 30$), while the 12-mer template resulted most frequently in values between the 10-, 11-, and 12-mer (Figure 3d and Table 1, $N > 10$). As shown in Table 1, the estimated diameters of pores from these assemblies were approximately 0.5 nm for tetramers, 2.3 nm for octamers, and 4.0 nm for dodecamers. Independent from

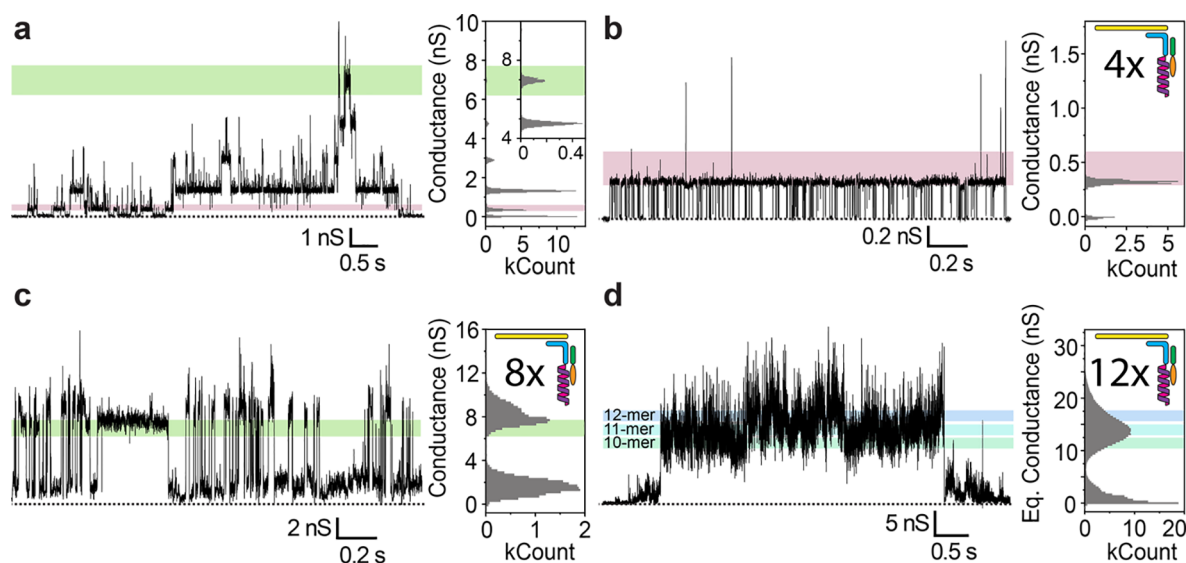


Figure 3. Templating DNA-modified CtxA peptides led to programmable pores with predominant pore diameters in planar lipid bilayer experiments. (a) Typical CtxA conductance levels observed for nontemplated Chol–dsDNA–CtxA (i.e., in the absence of a template strand). The shaded areas correspond to conductance levels of the 4-mer (O₂, pink) and 8-mer (O₆, green) as summarized in Table 1. (b) Presence of the 4-mer template led to a predominance of the conductance level of a 4-mer pore; larger pores were observed rarely (see corresponding histograms). (c) Presence of the 8-mer template led to large conductance steps directly to the conductance value for an 8-mer pore (note, the current scale is ~ 10 times larger than in b). (d) Presence of the 12-mer template generated large noise levels leading to rapid fluctuations in conductance between the levels that are consistent with those that would be recorded in the presence of pores formed by 12 ± 2 monomers (see histogram and shaded areas). All recordings were carried out with Chol–dsDNA–CtxA concentrations of 5 nM (a–c) or 20 nM (d) with applied potential differences of +180 mV (a,d), +160 mV (b), and +140 mV (c) using 1 M NaCl electrolyte solutions except for (d), which was carried out in 3 M CsCl in 30% (v/v) glycerol in water. In this case, we converted the conductance to the corresponding value in 1 M NaCl for comparison (see Supporting Information Section 3). In addition, we show in Supplementary Figures S5–S7 full 1 min recordings corresponding respectively to panels (b–d). Dotted lines correspond to 0 pA current.

these characterizations by electrical recordings in planar lipid bilayers, size exclusion chromatography confirmed the presence of tetrameric, octameric, and dodecameric assemblies in preparations with the respective template strands (see Supporting Information Section 5 and Supplementary Figures S11 and S12).

While the current traces in Figure 3 display the formation of pores with the programmed and desired size, we did not observe these results in all experiments. Specifically, we estimate that one-quarter to one-half of the experiments showed direct insertion of pores with the desired number of monomers or of pores with one monomer more or less than the size programmed by the template strand. The remaining experiments that did not show the expected single-step conductance variations displayed conductance increases in multiple steps, which were likely the results of step-by-step insertion of the templated monomers. We also observed pores with higher conductance values than expected, which may be caused by free CtxA monomers joining templated assemblies or multiple pores forming at the same time. We discuss the success rates of experiments in detail in Supporting Information Section 4.

Hydrophilic Modification on the C-Terminus of CtxA Peptides Stabilized the Pores. Applications such as resistive pulse recordings require long-lived pores with constant pore diameters in lipid or polymer membranes.^{7,50,51} To increase the lifetime of hybrid pores from CtxA–DNA, we covalently attached an additional hydrophilic segment consisting of 12 thymine nucleotides to the C-terminal part of the peptide (dsDNA–CtxA–T₁₂). We hypothesized that this T₁₂ segment might trap CtxA in a transmembrane

conformation once this C-terminal section inserts into, and crosses, the bilayer—in part because of its hydrophilicity and in part because of the favorable polarity of the applied potential difference (we added the dsDNA–CtxA–T₁₂ peptides to the *cis* compartment and polarized the *trans* compartment positively). Here, the idea was that a positive polarity in the *trans* compartment would facilitate the transfer of the negatively charged C-terminal T₁₂ segment through transient defects in the bilayer to achieve a transmembrane configuration of the peptide that is anchored on both sides of the membrane with DNA segments. Once the peptide adopted this configuration, we hypothesized that the T₁₂ segment on the *trans* side of the membrane may keep the peptide embedded stably in the membrane.

To test these hypotheses and to investigate the influence of the C-terminal T₁₂ segment on pore formation, we first added CtxA peptides modified on both termini in the absence of a template strand to the bilayer setup and recorded the current over time. We conducted such experiments more than 10 times. In more than half of the experiments, we recorded the presence of longer-lived pores (with the current remaining stable at the value of a specific open state for more than tens of seconds as opposed to hundreds of milliseconds for native CtxA or ssDNA–CtxA peptides that are not modified with the C-terminal T₁₂ segment). Due to the absence of the templating strand, the pore sizes that we recorded fluctuated significantly over the whole range of pore sizes (from 4-mers to 9-mers) rather than observing pentamers and hexamers as predominant pore sizes.^{38,41} Figure 4a–d shows single-step insertion of a pore formed by assembly of dsDNA–CtxA–T₁₂ monomers in a lipid membrane as well as its current–voltage curve.

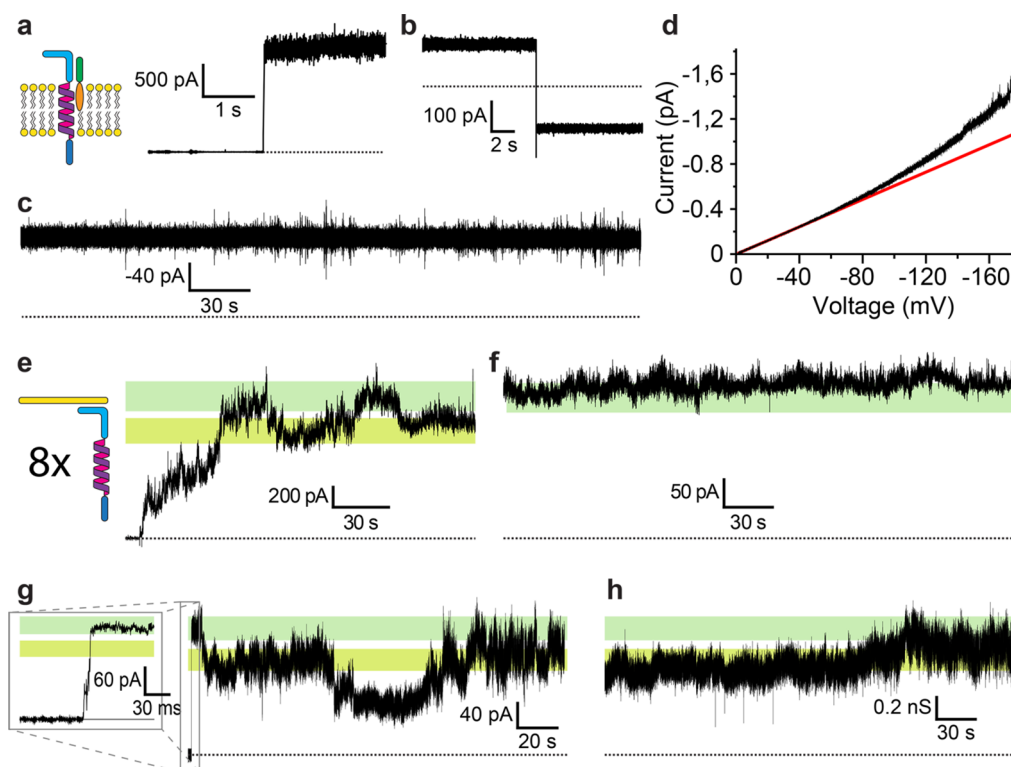


Figure 4. Formation of long-lived pores by CtxA peptides modified with DNA on both termini (dsDNA-CtxA-T₁₂). (a) Apparent single-step insertion of a single pore from nontemplated dsDNA-CtxA-T₁₂ peptides (applied potential: +180 mV). (b) The pore remained in the membrane after reversal of the voltage polarity from +20 to -20 mV. (c) Continuous, 5 min current recording showing a constant, uninterrupted open state of a pore formed by dsDNA-CtxA-T₁₂ peptides (applied voltage: -20 mV). (d) Current-voltage relationship of a long-lived single pore formed by dsDNA-CtxA-T₁₂ peptides. At increasing magnitudes of applied potential differences, the recorded current (black) deviated from linearity as indicated by the red line; CtxA pores are known to display nonlinear current-voltage behavior.³⁸ Panels (e,f) as well as panels (g,h) represent the insertion of DNA-modified peptides (dsDNA-CtxA-T₁₂) in the presence of the 8-mer template at +180 mV (e,g) and illustrate the relatively stable behavior of the octameric pore at a reduced voltage of +50 mV (f,h). Experiments were conducted in 1 M NaCl, 10 mM HEPES, pH 7.2, except for panels (g,f), for which we used 150 mM NaCl, 10 mM HEPES, pH 7.2. Shaded areas corresponding to conductance levels of the 7-mer (lime green) and 8-mer (mint green) are shown for comparison between the experiments. For clarity, each current trace was downsampled by a factor of 10 (except (d), which was downsampled 100 times, see [Supplementary Figure S15](#) for the current-voltage curve without downsampling). Dotted lines correspond to 0 pA current.

Estimated from the conductance value, this pore comprised eight or nine monomers, but we also observed long-lived pores consisting of four to seven monomers in similar experiments with dsDNA-CtxA-T₁₂ in the absence of a template strand as we show in [Supplementary Figure S17](#). [Figure 4a–d](#) demonstrates the persistence of this pore in the bilayer at low applied voltages. This pore formation at low voltage is unusual for a voltage-gated pore-forming peptide like CtxA or for its N-terminally modified DNA derivatives, because dipole-driven peptide insertion and pore formation usually only occur above a threshold voltage with favorable polarity.^{38,52} This voltage threshold, in the case of native CtxA, was typically between +140 and +180 mV for the peptide concentrations and experimental conditions we used. Furthermore, pores from CtxA peptides without the T₁₂ modification on their C-terminus typically closed rapidly after reversal of the voltage polarity to a *trans* negative potential. In contrast, pores from CtxA peptides with the C-terminal T₁₂ modification persisted not only at a single, stable conductance level for minutes (more than 25 min in the example shown in [Figure 4a–d](#)) while applying subthreshold *trans* positive polarities but also at the reverse polarity of *trans* negative potential differences ([Figure 4b–d](#)). CtxA peptides without the C-terminal T₁₂ modification, including native CtxA, in contrast, resulted in pores with

lifetimes of individual conductance states in the range of hundreds of milliseconds and, as stated above, closed almost instantly at *trans* negative potentials. Therefore, modification of the C-terminus with a hydrophilic and charged T₁₂ DNA segment prolonged the lifetime of open-pore conductance states by 3 orders of magnitude and enabled recordings at both polarities. One disadvantage of this strategy for pore stabilization, however, was that the wait time for pore formation with C-terminally T₁₂ modified CtxA peptides was sometimes significantly longer than with CtxA peptides without this modification. This prolonged waiting period could only be reduced somewhat by doubling or tripling the total peptide concentration.

To explore programmed assembly of CtxA peptides with C-terminal T₁₂ modification to long-lived pores of the desired size, we repeated the experiments with templated pores. To this end, we added purified octameric structures of dsDNA-CtxA-T₁₂ to the *cis* compartment and observed pore formation ([Figure 4e–h](#)). While the recorded current showed current fluctuations between the 7-mer and the 8-mer levels at the high voltage used for insertion (+180 mV, [Figure 4e,g](#)), reduction of the voltage to +50 mV resulted in improved stability of this octameric pore ([Figure 4f,h](#)). We obtained such long-lasting octamers in approximately one-third of the

experiments involving the 8-mer template ($N > 10$); in the remaining experiments, we observed long-lasting pores comprising fewer monomers than expected. Occasionally, we also observed transient fluctuations in conductance, which we attribute to one or a few peptide monomers leaving and joining the assembly.

Finally, in an attempt to increase the stability of DNA–CtxA pores further, we added the 8-mer templated dsDNA–CtxA– T_{12} to the *cis* compartment and templated the resulting pores also from the *trans* compartment by taking advantage of the T_{12} transmembrane ssDNA segment on the C-terminus of each CtxA peptide in the assembly (see Figure 5a,b). To do so, we hybridized an ssDNA oligonucleotide with 62 bases that included a complementary A_{12} segment on its 3' end. Like the oligonucleotide at the N-terminus of the peptide, this 62-base segment comprised a spacer region to circumvent steric hindrance during the assembly and a template-binding domain to trigger assembly to an 8-mer template. The template strand and the 62-base segment were preassembled and HPLC-purified before addition to the *trans* side of the lipid bilayer. We hypothesized that this approach would result in a pore structure that was templated on both sides of the bilayer and that such a double-templated pore would be more stable than a pore with one template on the N-terminal side of the peptides only.

Figure 5c shows the insertion of an octameric pore that was preassembled using DNA strands on the N-terminal side of CtxA. We added this assembly to the *cis* compartment, while the *trans* compartment contained the preassembled 8-mer DNA structure for templating the pore also on the C-terminal end of the peptide. The resulting double-templated pore led to a stable conductance level over more than 3 h of current recording (small current variations did occur after extended periods of times as represented by the current traces recorded after 2 h and after 3 h of pore insertion). Unfortunately, similar double-templating experiments conducted with 12-mer templates did, however, not improve pore stability compared to CtxA pore assemblies with one DNA template and were thus not pursued further. The results in Figure 5 with the 8-mer template, however, were consistent with the hypothesis that the presence of templating structures on both sides of the pore increases the stability of the pore assembly in the membrane. Figure 5 also shows that this approach renders the assembled pore less prone to fluctuations of the open-pore current than experiments without the second templating structure in the *trans* compartment (Figure 4e–h). Among the experiments with double-templated pores, we observed strongly improved stability in around 20% of the trials (out of $N = 12$ experiments, two experiments displayed the clear formation of stable pores with conductance values consistent with the formation of 8-mer pores), while the other experiments led to short-lived pores or long-lived but unstable pores, possibly due to the second templating structure not hybridizing in the adequate sequence to the pore assembly.

Altogether, the results in Figures 4 and 5 show that the hydrophilic C-terminal modification with T_{12} stabilized CtxA peptides in their transmembrane conformation. Adding an ssDNA template with a desired number of hybridization sites made it possible to define the size of the pores, while adding a second template strand together with an adaptor strand to the *trans* compartment further increased the stability and longevity of the pores. Modifying the transmembrane part of the CtxA peptide hence provides an attractive strategy for prolonging the

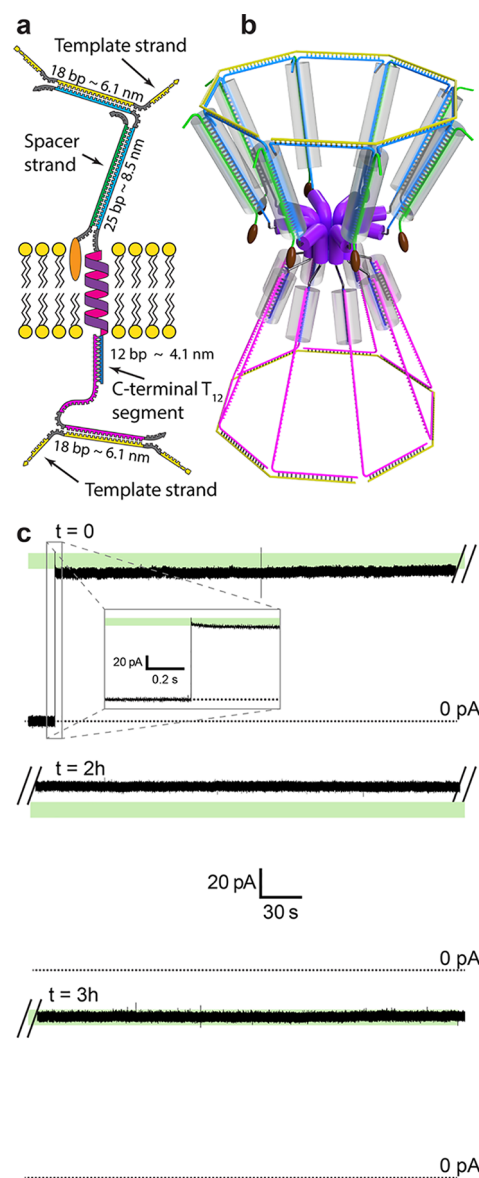


Figure 5. Formation of long-lived and stable pores by CtxA peptides that were templated on both sides of the membrane by hybridizing to an 8-mer template on the *cis* side and to an 8-mer template on the *trans* side of the planar lipid bilayer. (a) Cartoon of a dsDNA–CtxA– T_{12} monomer (purple) hybridized to a template strand (yellow) on both ends of the molecule. (b) Idealized representation of an octameric dsDNA–CtxA– T_{12} pore assembly templated from both sides of the lipid membrane. (c) Current versus time recordings after dsDNA–CtxA– T_{12} with an 8-mer template on the N-terminal end of the peptide was added to the *cis* side, while the *trans* side of the lipid bilayer contained a preassembled 8-mer template (yellow) with 12 adenine bases at the terminal end of its adaptor DNA strand (pink). This experiment resulted in stable pores at relatively high voltages (here +100 mV) and for more than 3 h. The lime green shaded area corresponds to the expected conductance level of an octameric pore. The recording buffer consisted of 150 mM NaCl, 10 mM HEPES, pH 7.2. The gray cylinders indicate the diameter of double-stranded DNA.

open state of pores from pore-forming peptides that otherwise fluctuate dynamically between conductance levels.

While the results in Figures 4 and 5 provide evidence for the programmed assembly of long-lived pores, our attempts to

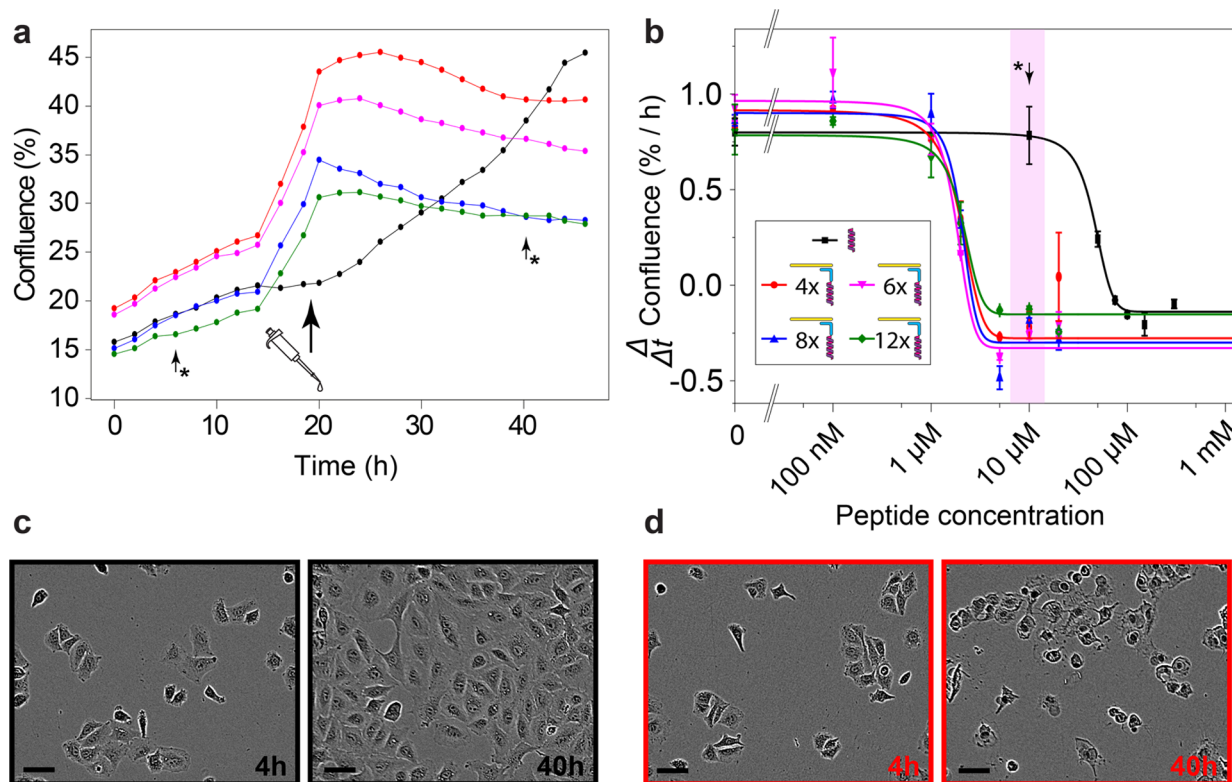


Figure 6. Cytotoxic activity of CtxA pores with various programmed diameters. (a) Confluence of cells in culture as a function of time before and after addition (large black arrow) of ssDNA–CtxA peptides that had been preassembled in the presence of ssDNA templates with 4 (red), 6 (pink), 8 (blue), or 12 (green) hybridization sites; data in black represents the control experiment with native CtxA in the absence of a template DNA. The total peptide concentration was $10\ \mu\text{M}$ in all cases. (b) Change in confluence over time as a function of the total peptide concentration of templated and nontemplated CtxA. (c) Phase-contrast micrographs taken shortly before (left image) and approximately 20 h after (right image) the addition of a $10\ \mu\text{M}$ monomeric nontemplated peptide for native CtxA peptides illustrating that cells continued to multiply and that the confluence of the cells increased after CtxA addition. (d) Phase-contrast micrographs taken shortly before (left image) and approximately 20 h after (right image) addition of tetrameric CtxA assemblies with a total peptide concentration of $10\ \mu\text{M}$ illustrating that cells stopped to multiply as well as assumed rounded shapes and that confluence stopped to increase after addition of tetramer assemblies or larger assemblies (b) of CtxA. The arrows and stars point out the concentrations or time points used as examples in the different panels. The images shown in (c,d) correspond to the area shaded in pink in (b). Scale bars: $50\ \mu\text{m}$.

observe translocations of small polymer molecules through these pores with a single template (Figure 4) or with two templates (Figure 5) were unfortunately not successful. We performed these experiments with a mixture of polymers, including PEG 200, PEG 1500, PEG 4000, and dextran sulfate 8000 present in a concentration range from 30 to $920\ \mu\text{M}$ on both sides of the membrane while conducting recordings at a range of applied voltages between -200 and $+200\ \text{mV}$. While we could not detect resistive pulses in most experiments, a few experiments did lead to resistive pulse-like signals (see Supplementary Figure S18); due to the low success rate of these experiments, we could, however, not confirm with certainty that these signals were indeed arising from the translocation of the polymers or from fluctuations of a pore that was unstable during these recordings. The amplitude of some of these resistive pulses was in a similar range as transitions from an 8-mer pore to a 7-mer pore; other pulses, however, had bigger amplitudes that could be consistent with polymer translocations.

A potential explanation for the lack of clearly attributable translocation events could be that the molecular structure of the DNA template above the pore (Figure 1c–e) impeded the entry of polymers into the pore, for instance by folding in such a way that DNA strands interacted with the pore entrance. The

cartoons of the assembly in Figure 1c–e are idealized representations; due to the flexibility of the short ssDNA T_4 segments, many other conformations of the DNA template structure are plausible, some of which might be stabilized by interactions of the negatively charged DNA structure with amino acids on the N-terminus of CtxA, in particular since these include at least four positively charged lysine residues. Such interactions may sterically block the translocation of polymers while permitting the permeation of ions though the pore and thus only exerting a small effect on the measured conductance. Another explanation could be that the recorded and stable open-pore currents did not result from the desired DNA-programmed assembly of a single octameric pore but rather from two hexameric pores, four to five pentameric pores, or any other combination of smaller pores leading to a similar total conductance as an octameric pore. This scenario is, however, not likely as the majority of the pores we observed incorporated in the bilayer with a single-step current increase—to the conductance value of an octameric pore assembly as shown in Figures 3b,c, 4a, and 5. Moreover, the likelihood for one stable open channel conductance over extended periods of time decreases with increasing numbers of simultaneously open independent pores in the bilayer; the

long-term stabilities of the open-pore currents in Figures 4e,f and 5 are therefore most consistent with a single octameric pore.

Template-Assembled CtxA Pores Prevented the Proliferation of Cancer Cells at Lower Total Peptide Concentration than Native CtxA. We hypothesized that DNA templating of ssDNA–CtxA to form preassembled pores may enhance the toxicity of the peptides for applications of targeted cell killing compared to exposure of cells to the same total concentration of CtxA peptides in the absence of a template. Naturally, the antimicrobial peptide CtxA is produced by the medfly *Ceratitis capitata* in order to protect its eggs.⁵³ As the cytotoxicity of pore-forming antimicrobial peptides correlates with pore size and peptide concentration,³⁸ we hypothesized that templated CtxA peptides would be more cytotoxic than nontemplated CtxA peptides due to the increased local peptide concentration and formation of larger pores.³⁸

To investigate the cytotoxic activity of DNA-templated CtxA peptides, we monitored the growth of the epithelial lung cancer cell line A549 upon addition of 4-, 6-, 8-, and 12-mer templated CtxA peptides and compared it to the growth of these cells after adding native CtxA as control. As a metric for cell viability, we determined the change in confluence of the cells as a function of time for a range of total peptide concentrations. Figure 5 shows that concentrations of 50 to 100 μM of native CtxA were necessary to stop cell proliferation. In the case of the DNA-templated assemblies of CtxA, less than 5 μM of total CtxA concentration was sufficient to completely stop the proliferation of the same cells and to induce a dramatic change in the shape of these cells to a small, rounded cell shape that is typical for dying or dead cells (Figure 6d).⁵⁴ Similar toxicity required 100–150 μM of native CtxA and hence a more than 20-fold higher total peptide concentration compared to templated CtxA peptides. Surprisingly, all templated assemblies of CtxA, from tetramers to dodecamers, required similar total peptide concentrations to induce their cytotoxic effect. This observation could be in part explained by the fact that we plotted the total CtxA peptide concentration instead of the concentration of assemblies; indeed, for a given total peptide concentration, more tetrameric assemblies will be formed than dodecameric assemblies. When we expressed the concentration of the assembled structure rather than the total peptide concentration and compared the effect of the dodecameric assembly to the tetrameric assembly or to native CtxA as three potential drug candidates, then each 12-mer assembly was approximately 3 times more toxic than each 4-mer assembly and approximately 200 times more toxic than each CtxA molecule. In other words, 420 nM of an assembled 12-mer reduced viability to a similar extent as 100 μM native CtxA.

CONCLUSION

The design, synthesis, and assembly of artificial functional proteins has long been one of the most challenging goals in protein biochemistry. The work presented here explored the potential of DNA nanotechnology to develop a modular strategy for the programmed self-assembly of pore-forming peptides to functional transmembrane pores with adjustable diameters, membrane affinity, and open-pore lifetimes. The resulting assemblies of tetrameric, octameric, and dodecameric supramolecular structures made it possible to favor the formation of predefined pores with estimated inner pore

diameters of approximately 0.5, 2.3, and 4.0 nm. Functionalization of these peptide–DNA hybrids with a cholesterol-bearing DNA strand significantly increased their affinity to the lipid membrane as well as their propensity to adopt well-defined conductance states. Among the templated pores that we assembled, the tetrameric and octameric assemblies formed the most stable pores, while the conductance levels of the dodecameric pores often fluctuated between those levels of 9-mer to 13-mer assemblies. Further modification aiming at stabilizing the peptides in the membrane-spanning conformation by modifying the C-terminal end of CtxA with a hydrophilic T₁₂ DNA segment, prolonged the open-state lifetime of the assembled pores from milliseconds to minutes at one stable and constant conductance level. Hybridization of a second DNA template strand to the C-terminus of CtxA further stabilized the pores, leading, in some experiments, to constant conductance levels that persisted for hours.

This work demonstrates that the programmed assembly of hybrid DNA–peptide nanostructures to transmembrane pores incurs at least six attractive characteristics. First is the ability to fine-tune the pore diameter in increments of individual, α -helical peptides with low molecular weight by self-assembly onto readily available ssDNA templates. Second is the presence of an open DNA-based scaffold that circumvents additional electrical resistance from a tightly packed vestibule. Third is the applicability of sequence-specific orthogonal hybridization chemistry for modifying defined positions in the structure, for instance with a cholesterol anchor, fluorophore, or targeting moiety.⁴ Fourth is the accessibility, scalability, and robustness of the approach based on straightforward design that requires only three different molecules (ssDNA template, ssDNA–CtxA, ssDNA–Chol) that can all be obtained from commercial sources. Fifth is the production of CtxA peptides by solid-phase synthesis, making modifications or functionalization of individual amino acids at precisely defined locations straightforward. And sixth is the possibility to kill cancer cells in culture at 20-fold lower total peptide concentrations compared to nontemplated CtxA peptides. Future extensions of this work may target specific cell types,⁴ pathogens, or analytes by functionalizing the constructs with ssDNA-tagged ligands, antibodies, or aptamers.

One of the biggest challenges in the programmed assembly of nanopores from pore-forming peptides or proteins appears to be the capability of these pores to enable the translocation of macromolecules through their lumen. In fact, we are not aware of a demonstration of recorded resistive pulses through an artificially templated pore assembly. The two pioneering studies on DNA-programmed pore assembly^{22,37} also did not demonstrate the translocation of analytes and did not include a discussion if and why achieving translocation may be difficult. In the work presented here, we consider two possible reasons for this difficulty: first, fast fluctuations of peptides on time scales that cannot be resolved (i.e., nanoseconds or microseconds), might increase the entropic barrier for the entry of macromolecules into the pore lumen. And second, electrostatic interactions between the negatively charged DNA structure and positively charged lysine side chains on the N-terminal end of all CtxA peptides in the assembly may position DNA strands across the opening of the pore without significantly reducing the ionic current through the pore. In addition, when the polarity of the applied transmembrane voltage is positive in the *trans* compartment (as is favorable for the formation of pores from CtxA peptides that were added to the *cis* compartment),

then the short-range electric field that extends from the pore entrance would also attract negatively charged DNA toward the entrance of the pore. These effects might block the entry of macromolecules while having only a small effect on the passage of ions through the pores. Future designs of programmable, DNA-templated nanopores may therefore benefit from a DNA structure that is overall more rigid²² and that is connected to the pore-forming peptides with a more rigid attachment than the one we used. In comparison, the structure presented here was designed to be flexible by incorporation of four single-stranded thymidine nucleotides between each binding site on the template and between each N-terminus of CtxA and the covalently attached DNA strand.

While the work presented here did not yet produce hybrid DNA–peptide nanopores that could be used for resistive pulse experiments, it demonstrated proof-of-principle for programmed assembly of nanopores with tunable diameter that have the capability to self-incorporate into lipid bilayer membranes—this capability is an advantage compared to many natural ion channel proteins that do not spontaneously self-incorporate into lipid membranes from solution but rather require cumbersome and often inefficient reconstitution protocols such as the fusion of proteoliposomes into lipid bilayers.⁵⁵ To our knowledge, the approach presented here enabled the largest templated assembly of pore-forming peptides—as opposed to pore-forming proteins³⁷—to a functional pore reported to date. These templated pores showed significantly increased cytotoxicity in a cancer cell line compared to the same total peptide concentration of native CtxA and may become useful as gateways for targeted drug delivery, single-cell biopsy, or targeted cell killing.

MATERIALS AND METHODS

Materials. We purchased all lipids (1-palmitoyl-2-oleoyl-*sn*-glycero-3-phosphocholine (POPC), 1,2-dioleoyl-*sn*-glycero-3-phosphoethanolamine (DOPE), 1-palmitoyl-2-oleoyl-*sn*-glycero-3-phospho-L-serine (sodium salt) (POPS), and 1,2-diphytanoyl-*sn*-glycero-3-phosphocholine (DiPhyPC)) from Avanti Polar Lipids (Alabaster, AL, USA). CtxA (purity > 98%), ssDNA–CtxA (purity > 92%), ssDNA–CtxA–azide (purity > 98%), and azide–CtxA–SH (purity > 98%) were synthesized and purified by Bio-Synthesis Inc. (Lewisville, TX, USA). The certificates of analysis with the corresponding mass spectra and HPLC reports from the supplier can be found in [Supporting Figures S23 to S31](#). We acquired the DNA oligonucleotides for the template strands and the spacer strands—with and without cholesterol—from Biomers (Ulm, Germany), Eurofins (Eurofins MWG, Ebersberg, Germany, HPSF purification), Jena Bioscience (Jena, Germany), and Metabion (Planegg/Steinkirchen, Germany). We solubilized all chemicals either in pure water or in Tris-EDTA buffer (TE buffer, 10 mM Tris-HCl, 1 mM disodium EDTA, pH 8.0). We purchased all other chemicals from Sigma-Aldrich (St. Louis, MO, USA). We purchased all material for the HPLC, e.g., size exclusion chromatography (AT-5190-2503) and strong anion exchange (AT-5190-2467) columns, 1.5 mL glass vials (LP-11090477) and inserts for low volumes (LPP06 09 0357) for sample injection, and 1.5 mL glass vials (AT-5182-0716) with screw caps (AT-5190-7024) for fraction collection, from BGB Analytik SA (Geneva, Switzerland). We purchased crim caps with a PTFE/silicon septum (Art. LC26.1) for 1.5 mL glass vials from Carl Roth Switzerland.

Planar Lipid Bilayer Recordings. The lipid composition of most bilayers consisted of POPC, DOPE, and POPS with a 7:3:1 (w/w) ratio except for the experiments with 8-mer templated dsDNA–CtxA–T₁₂ for which we used pure DiPhyPC lipids to increase the membrane stability. We dissolved all lipid mixtures in pentane at a total lipid concentration of 10 mg/mL. We used three buffered

electrolyte solutions containing either 1 M or 150 mM NaCl with 10 mM HEPES buffer at a pH 7.2–7.3 or 3 M CsCl, 10 mM HEPES, pH 7.4, in 30% (v/v) glycerol in water. We filtered the electrolyte solutions with 0.2 μ m poly(ether sulfone) filters (VWR, Radnor, PA, USA) before use. For the translocation experiments, we used a mixture containing 70 μ M PEG 200, 920 μ M PEG 1500, 460 μ M PEG 4000, and 30 μ M dextran sulfate.

We defined the *cis* compartment of the recording setup as the compartment where we added the peptides; this compartment was connected electrically to the ground. We defined the voltage and its polarity by connecting the headstage of the amplifier to the *trans* compartment. We placed the Teflon chambers inside Faraday cages, on a BM4 vibration isolation platform (Minus K Technology, Inc., Inglewood, CA, USA). We carried out all experiments at room temperature (22 ± 1 °C). We used three different amplifiers (BC-535, Warner Instruments Hamden, CT, USA; EPC7, HEKA Instruments Inc., Holliston, MA, USA; or eOne HS, Elements, Cesena, Italy). We filtered the recorded currents with a built-in low-pass filter using a cutoff frequency of 10 kHz for the BC-535 and EPC7 or 6.25 kHz for the templated 12-mer data gathered with the eOne and sampled all data at 50 kHz. We analyzed data using OriginLab (OriginLab Corporation, Northampton, MA, USA) and pClamp (Molecular Devices, Sunnyvale, CA, USA) software. See [Supporting Information Section 7](#) for details.

Formation of the Membranes. We used Teflon chambers with two compartments with maximum volumes of 1.5 mL and 200 μ L. We pretreated Teflon films (Eastern Scientific LLC, Rockville, MD) with apertures of 50 μ m by pipetting 1 μ L of pretreatment solution—hexadecane 5% (v/v) in hexane—onto both sides of the aperture of the Teflon film. We then mounted the Teflon film in a Teflon chamber using high-vacuum grease (Dow Corning Corporation), separating the two compartments of the Teflon chamber, and formed planar lipid bilayers using the technique described by Montal and Mueller.⁵⁶ Briefly, we added electrolyte solution to both compartments (1.3 mL in the big compartment and 180 μ L for the smaller one) and spread 1–2 μ L of lipid solution onto the surface of the buffered electrolyte solution. After the solvent evaporated, a lipid monolayer (Langmuir film) formed at the air–water interface. We raised and lowered the electrolyte solution until we measured a baseline current ($-3 < I < 3$ pA) indicating that a bilayer had formed. We then thinned the membrane by lowering and raising the electrolyte solution in one compartment, until we measured a capacitance of 60 ± 10 pF. To monitor capacitance, we applied a triangular voltage, and the capacitance was either calculated by the amplifier or determined using the manual capacitance compensation of the amplifier. Prior to adding the peptide, we checked the stability of the bilayer (absence of leak currents, expected noise level) by applying transmembrane voltages of up to 200 mV for 5 min at both polarities.

Formation of the Assemblies. We conducted all the experiments with the 4-mer or 8-mer templates (with a single templating structure on the N-terminus of CtxA) without purification except for 8-mer templated dsDNA–CtxA–T₁₂, which we purified using size exclusion high performance liquid chromatography (SEC-HPLC). We added ssDNA–CtxA and the spacer strand stoichiometrically and added the 4- or 8-mer template at a ratio of 1 mol for 5 mol of DNA-modified peptide for the 4-mer or 10 mol of DNA-modified peptide for the 8-mer templates and prepared them following two different methods. In one method, we added all components with nM concentrations directly in the recording chamber sequentially, first ssDNA–CtxA followed by either the template strand or spacer (with or without cholesterol) strand, one after the other. Alternatively, we mixed the ssDNA–CtxA with the template and spacer (with or without cholesterol) strands in a DNA LoBind tube (Eppendorf Tubes, Hamburg, Germany) and let them react overnight at room temperature. We reacted all the components in micromolar concentrations and later diluted the samples prior to adding them to the buffered electrolyte solution.

We purified the 12-mer assemblies of Chol–dsDNA–CtxA and the 8-mer assemblies of dsDNA–CtxA–T₁₂ using SEC-HPLC, with an

Agilent SEC3 column (300 mm length, 300 nm pore size, 4.6 mm internal diameter) using 1× PBS + 1 mM EDTA as the running buffer at a flow rate of 0.3 mL/min. These assemblies were preincubated according to the following procedure: in an Eppendorf tube, we mixed ssDNA–CtxA or dsDNA–CtxA–T₁₂ in excess (>4 DNA–peptide monomers per binding site on the template strand) with the template strands. We added Milli-Q water and NaCl from a 5 M NaCl stock solution in order to reach a final NaCl concentration of 1 M. We hybridized the mixture overnight at 22 °C while mixing gently with a thermomixer. During purification, we collected the fractions containing the full assemblies to remove the excess monomers and stored them at +4 °C for later use.

The second templating structure for the experiments with double-templated octameric dsDNA–CtxA–T₁₂ pores was preassembled according to the following procedure: in an Eppendorf tube containing the 8-mer template strands, we added the DNA strands that were designed to bind on one end to the template and on the other end to the T₁₂ segment on the C-terminus of dsDNA–CtxA–T₁₂ in excess (>4 DNA strands per binding site on the template strand). We then added Milli-Q water and NaCl from a 5 M NaCl stock solution in order to reach a final NaCl concentration of 1 M. We left the mixture to hybridize overnight under gentle agitation, at 22 °C in a thermomixer and purified it by SEC-HPLC to obtain a solution with the 8-mer assembly (but without free DNA strands) for further use as the second templating structure in the *trans* compartment of the lipid bilayer setup.

While we ordered ssDNA–CtxA with the CtxA peptide and the ssDNA oligonucleotide covalently linked, we prepared dsDNA–CtxA–T₁₂ ourselves. To do so, we followed two reaction routes. For the experiments with single templates (corresponding to Figure 4a–f), we prepared dsDNA–CtxA–T₁₂ molecules by reacting ssDNA–CtxA–azide (Bio-Synthesis Inc., purity > 98%) with an excess of a 12-base oligonucleotides modified on their 5′ end by a dibenzocyclooctyne (DBCO) group (12T-DBCO), at 22 °C under mild shaking, followed by subsequent SEC-HPLC purification to remove the excess, unreacted species. Alternatively, experiments with CtxA peptides templated from both ends required the use of CtxA peptides modified by an azide group on CtxA’s N-terminus and a thiol (–SH) group on the C-terminal end (Az–CtxA–SH). Preliminary experiments using SEC-HPLC revealed that Az–CtxA–SH was mostly present in solution in monomeric form. The presence of dimers that would be formed through disulfide bridges between two Az–CtxA–SH peptide monomers was negligible (data not shown), but in the case the number of dimers had increased, we always added Az–CtxA–SH in excess compared to the DNA oligonucleotide that reacted with the peptide (>5 Az–CtxA–SH compared to the DNA oligonucleotide).

First, we incubated Az–CtxA–SH with a 12-base oligonucleotide consisting of 12 thymine bases with a maleimide activation on its 5′ end (12T-Mal) by adding Az–CtxA–SH in a >5-fold excess compared to 12T-Mal overnight, under gentle agitation, at 22 °C on a thermomixer. We purified the reacted Az–CtxA–T₁₂ using an Agilent strong anion exchange (SAX) column (250 mm length, 5 μm particle size, 4.6 mm internal diameter) with a flow rate of 0.5 mL/min. The CtxA peptide being positively charged, it is not retained by the SAX column, and only the unreacted DNA oligonucleotides and the DNA-modified peptides are retained. We applied an elution profile with a linear gradient from 0 to 100%B in 20 min, with mobile phase A consisting of 20% acetonitrile (v/v) in water and mobile phase B consisting of 2 M ammonium formate dissolved in 20% acetonitrile (v/v) in water (see Supplementary Figure S21, inset of panel A for the gradient elution profile). After the 20 min gradient, we left the flow to 100% B to wash the column for 2 min, followed by 13 min with 0% B for re-equilibration of the column for the next run. Subsequent SAX-HPLC analyses confirmed the absence of free Az–CtxA–SH peptides and free 12T-Mal oligonucleotides in the collected samples (see Supplementary Figure S21A). We then put all collected samples in a SpeedVac (Savant SPD111 V, Thermo Scientific) overnight until complete evaporation of the water and the ammonium formate and calculated the concentration of the collected samples (see Supplementary Section S8).

As a second step, we reacted the purified Az–CtxA–T₁₂ molecules with DBCO-modified ssDNA oligonucleotides (DNA–DBCO) with the same sequence that we used for the ordered ssDNA–CtxA peptides. We added Az–CtxA–T₁₂ in a 3- to 5-fold excess compared to DNA–DBCO and left it overnight, under gentle agitation, at 22 °C on a thermomixer. We purified the reacted ssDNA–CtxA–T₁₂ (see Supplementary Figure S21B for the collected molecules) using the same SAX column as for the first reaction step, with the same flow rate (0.5 mL/min), mobile phases (20% acetonitrile (v/v) in water and 2 M ammonium formate dissolved in 20% acetonitrile (v/v) in water), and gradient (0 to 100% B). Subsequent SAX-HPLC analyses confirmed the absence of unreacted Az–CtxA–T₁₂ or DNA–DBCO molecules. We then put all collected samples in a SpeedVac overnight until complete evaporation of the water and the ammonium formate and calculated the concentration of the collected samples (see Supplementary Section S9).

The last reaction step consisted of the hybridization of the purified ssDNA–CtxA–T₁₂ with the template of interest (mostly the 8-mer template for these experiments) as described above.

The 4-, 6-, 8-, and 12-mer assemblies for cytotoxicity experiments were prepared by mixing ssDNA–CtxA with each template stoichiometrically—with a ratio of 1 mol of a 4-, 6-, 8- or 12-mer template for 4, 6, 8, or 12 mol of DNA-modified peptide—to maximize the amount of templated assemblies while minimizing the amount of free ssDNA–CtxA peptide hybrids. We did not purify, as our SEC-HPLC conditions would introduce salts into the templated peptide solution, which could affect the viability of the cells.

For planar lipid bilayer recordings of purified structures with the cholesterol strand, we heated the ssDNA–cholesterol for 5 min at +60 °C before reacting it in a 5- to 10-fold excess with purified assemblies of ssDNA–CtxA to minimize aggregation of the cholesterol moieties. See Supporting Information Section 7 for details.

Cell Culture Experiments. We grew lung epithelial A549 cells in RPMI 1640 medium containing 25 mM HEPES, 1% L-glutamine, and 10% fetal bovine serum and added 1% penicillin–streptomycin for prevention of bacterial contamination of cell cultures. We seeded the cells in 96-well plates (TPP, Trasadingen, Switzerland) with 10 000 cells per well, in a total volume of 50 μL per well. We placed the plates in the IncuCyte Zoom imaging system (Essen Bioscience, Ann Arbor, MI, USA) inside of an incubator set to 37 °C and 5% CO₂ and monitored the growth of the cells by analyzing the change in confluence over time as provided by the IncuCyte software.

We seeded the cells and left them to adhere and replicate for 20 h before adding the templated CtxA–DNA 4-, 6-, 8-, and 12-mer assemblies or native CtxA as controls. We then measured the cell confluence every 2 h. To estimate the effect of the different peptide assemblies on the change in confluence over time, we fitted the observed confluence levels between 28 to 50 h linearly (corresponding to 8 to 30 h after peptide addition) and reported the slopes of the fits (See Supporting Information Section 6 for more details).

ASSOCIATED CONTENT

Supporting Information

The Supporting Information is available free of charge at <https://pubs.acs.org/doi/10.1021/acsnano.0c10311>.

HPLC chromatograms, chemical structures, additional current traces, fitting parameters for cell culture experiments (PDF)

AUTHOR INFORMATION

Corresponding Author

Michael Mayer – Adolphe Merkle Institute, University of Fribourg, 1700 Fribourg, Switzerland;
Email: michael.mayer@unifr.ch

Authors

Aziz Fennouri – Adolphe Merkle Institute, University of Fribourg, 1700 Fribourg, Switzerland; orcid.org/0000-0003-0922-2745

Jonathan List – Adolphe Merkle Institute, University of Fribourg, 1700 Fribourg, Switzerland; Present Address: Physics of Synthetic Biological Systems, Technical University Munich, Am Coulombwall 4a, 85748 Garching, Germany. (J.L.); orcid.org/0000-0001-8408-0877

Julie Ducrey – Adolphe Merkle Institute, University of Fribourg, 1700 Fribourg, Switzerland

Jessica Dupasquier – Adolphe Merkle Institute, University of Fribourg, 1700 Fribourg, Switzerland

Viktorija Sukyte – Adolphe Merkle Institute, University of Fribourg, 1700 Fribourg, Switzerland

Simon F. Mayer – Adolphe Merkle Institute, University of Fribourg, 1700 Fribourg, Switzerland

Reyner D. Vargas – Adolphe Merkle Institute, University of Fribourg, 1700 Fribourg, Switzerland

Laura Pascual Fernandez – Adolphe Merkle Institute, University of Fribourg, 1700 Fribourg, Switzerland

Frederick Bertani – Adolphe Merkle Institute, University of Fribourg, 1700 Fribourg, Switzerland

Sandra Rodriguez Gonzalo – Adolphe Merkle Institute, University of Fribourg, 1700 Fribourg, Switzerland

Jerry Yang – Department of Chemistry and Biochemistry, University of California, San Diego, California 92093, United States; orcid.org/0000-0002-8423-7376

Complete contact information is available at:
<https://pubs.acs.org/10.1021/acsnano.0c10311>

Author Contributions

[‡]A.F. and J.L. contributed equally.

Notes

The authors declare the following competing financial interest(s): A.F., J.L., and M.M. have filed a patent (applicant: Adolphe Merkle Institute, University of Fribourg) covering oligonucleotide-based tuning of pore-forming peptides (EP2019076974W filed 2019-10-04 claiming priority of US201862742579P filed 2018-10-08).

ACKNOWLEDGMENTS

Funding: This work was supported by the Swiss National Science Foundation through the National Centre of Competence in Research Bio-Inspired Materials (grant number 51NF40-141849). We thank Stefano Vanni for discussions and Laurent Mène-Saffrané for support with purification of the assemblies.

REFERENCES

- (1) Kasianowicz, J. J.; Brandin, E.; Branton, D.; Deamer, D. W. Characterization of Individual Polynucleotide Molecules Using a Membrane Channel. *Proc. Natl. Acad. Sci. U. S. A.* **1996**, *93* (24), 13770–13773.
- (2) Howorka, S.; Siwy, Z. Nanopore Analytics: Sensing of Single Molecules. *Chem. Soc. Rev.* **2009**, *38* (8), 2360–2384.
- (3) Oukhaled, A.; Bacri, L.; Pastoriza-Gallego, M.; Betton, J.-M.; Pelta, J. Sensing Proteins through Nanopores: Fundamental to Applications. *ACS Chem. Biol.* **2012**, *7* (12), 1935–1949.
- (4) Majd, S.; Yusko, E. C.; Billeh, Y. N.; Macrae, M. X.; Yang, J.; Mayer, M. Applications of Biological Pores in Nanomedicine, Sensing, and Nanoelectronics. *Curr. Opin. Biotechnol.* **2010**, *21* (4), 439–476.

- (5) Kasianowicz, J. J.; Balijepalli, A. K.; Ettetdgui, J.; Forstater, J. H.; Wang, H.; Zhang, H.; Robertson, J. W. F. Analytical Applications for Pore-Forming Proteins. *Biochim. Biophys. Acta, Biomembr.* **2016**, *1858* (3), 593–606.

- (6) Butler, T. Z.; Pavlenok, M.; Derrington, I. M.; Niederweis, M.; Gundlach, J. H. Single-Molecule DNA Detection with an Engineered MspA Protein Nanopore. *Proc. Natl. Acad. Sci. U. S. A.* **2008**, *105* (52), 20647–20652.

- (7) Morton, D.; Mortezaei, S.; Yemenicioglu, S.; Isaacman, M. J.; Nova, I. C.; Gundlach, J. H.; Theogarajan, L. Tailored Polymeric Membranes for Mycobacterium Smegmatis Porin A (MspA) Based Biosensors. *J. Mater. Chem. B* **2015**, *3* (25), 5080–5086.

- (8) Soskine, M.; Biesemans, A.; Moeyaert, B.; Cheley, S.; Bayley, H.; Maglia, G. An Engineered ClyA Nanopore Detects Folded Target Proteins by Selective External Association and Pore Entry. *Nano Lett.* **2012**, *12* (9), 4895–4900.

- (9) Soskine, M.; Biesemans, A.; De Maeyer, M.; Maglia, G. Tuning the Size and Properties of ClyA Nanopores Assisted by Directed Evolution. *J. Am. Chem. Soc.* **2013**, *135* (36), 13456–13463.

- (10) Wendell, D.; Jing, P.; Geng, J.; Subramaniam, V.; Lee, T. J.; Montemagno, C.; Guo, P. Translocation of Double-Stranded DNA through Membrane-Adapted phi29 Motor Protein Nanopores. *Nat. Nanotechnol.* **2009**, *4* (11), 765–772.

- (11) Huang, G.; Willems, K.; Soskine, M.; Wloka, C.; Maglia, G. Electro-Osmotic Capture and Ionic Discrimination of Peptide and Protein Biomarkers with FraC Nanopores. *Nat. Commun.* **2017**, *8* (1), 935.

- (12) Huang, G.; Voet, A.; Maglia, G. FraC Nanopores with Adjustable Diameter Identify the Mass of Opposite-Charge Peptides with 44 Da Resolution. *Nat. Commun.* **2019**, *10* (1), 835.

- (13) Goyal, P.; Krasteva, P. V.; Van Gerven, N.; Gubellini, F.; Van den Broeck, I.; Troupiotis-Tsailaki, A.; Jonckheere, W.; Péhau-Arnaudet, G.; Pinkner, J. S.; Chapman, M. R.; Hultgren, S. J.; Howorka, S.; Fronzes, R.; Remaut, H. Structural and Mechanistic Insights Into the Bacterial Amyloid Secretion Channel CsgG. *Nature* **2014**, *516*, 250.

- (14) Stefureac, R.; Long, Y.-t.; Kraatz, H.-B.; Howard, P.; Lee, J. S. Transport of α -Helical Peptides through α -Hemolysin and Aerolysin Pores. *Biochemistry* **2006**, *45* (30), 9172–9179.

- (15) Fennouri, A.; Przybylski, C.; Pastoriza-Gallego, M.; Bacri, L.; Auvray, L.; Daniel, R. Single Molecule Detection of Glycosaminoglycan Hyaluronic Acid Oligosaccharides and Depolymerization Enzyme Activity Using a Protein Nanopore. *ACS Nano* **2012**, *6* (11), 9672–9678.

- (16) Cao, C.; Ying, Y.-L.; Hu, Z.-L.; Liao, D.-F.; Tian, H.; Long, Y.-T. Discrimination of Oligonucleotides of Different Lengths with a Wild-Type Aerolysin Nanopore. *Nat. Nanotechnol.* **2016**, *11*, 713.

- (17) Merstorf, C.; Cressiot, B.; Pastoriza-Gallego, M.; Oukhaled, A.; Betton, J.-M.; Auvray, L.; Pelta, J. Wild Type, Mutant Protein Unfolding and Phase Transition Detected by Single-Nanopore Recording. *ACS Chem. Biol.* **2012**, *7* (4), 652–658.

- (18) Howorka, S.; Bayley, H. Probing Distance and Electrical Potential within a Protein Pore with Tethered DNA. *Biophys. J.* **2002**, *83* (6), 3202–3210.

- (19) Chavis, A. E.; Brady, K. T.; Hatmaker, G. A.; Angevine, C. E.; Kothalawala, N.; Dass, A.; Robertson, J. W. F.; Reiner, J. E. Single Molecule Nanopore Spectrometry for Peptide Detection. *ACS Sensors* **2017**, *2* (9), 1319–1328.

- (20) Wolfe, A. J.; Mohammad, M. M.; Cheley, S.; Bayley, H.; Movileanu, L. Catalyzing the Translocation of Polypeptides through Attractive Interactions. *J. Am. Chem. Soc.* **2007**, *129* (45), 14034–14041.

- (21) Howorka, S.; Cheley, S.; Bayley, H. Sequence-Specific Detection of Individual DNA Strands Using Engineered Nanopores. *Nat. Biotechnol.* **2001**, *19* (7), 636.

- (22) Spruijt, E.; Tusk, S. E.; Bayley, H. DNA Scaffolds Support Stable and Uniform Peptide Nanopores. *Nat. Nanotechnol.* **2018**, *13* (8), 739–745.

- (23) Rothmund, P. W. Folding DNA to Create Nanoscale Shapes and Patterns. *Nature* **2006**, *440* (7082), 297–302.
- (24) Ke, Y.; Ong, L. L.; Shih, W. M.; Yin, P. Three-Dimensional Structures Self-Assembled from DNA Bricks. *Science* **2012**, *338* (6111), 1177–83.
- (25) Douglas, S. M.; Marblestone, A. H.; Teerapittayanon, S.; Vazquez, A.; Church, G. M.; Shih, W. M. Rapid Prototyping of 3D DNA-Origami Shapes with caDNA. *Nucleic Acids Res.* **2009**, *37* (15), 5001–6.
- (26) Douglas, S. M.; Bachelet, I.; Church, G. M. A Logic-Gated Nanorobot for Targeted Transport of Molecular Payloads. *Science* **2012**, *335* (6070), 831–4.
- (27) Benson, E.; Mohammed, A.; Gardell, J.; Masich, S.; Czeizler, E.; Orponen, P.; Hogberg, B. DNA Rendering of Polyhedral Meshes at the Nanoscale. *Nature* **2015**, *523* (7561), 441–4.
- (28) Langecker, M.; Arnaut, V.; Martin, T. G.; List, J.; Renner, S.; Mayer, M.; Dietz, H.; Simmel, F. C. Synthetic Lipid Membrane Channels Formed by Designed DNA Nanostructures. *Science* **2012**, *338* (6109), 932–6.
- (29) Krishnan, S.; Ziegler, D.; Arnaut, V.; Martin, T. G.; Kapsner, K.; Henneberg, K.; Bausch, A. R.; Dietz, H.; Simmel, F. C. Molecular Transport through Large-Diameter DNA Nanopores. *Nat. Commun.* **2016**, *7*, 12787.
- (30) Gopfrich, K.; Li, C. Y.; Ricci, M.; Bhamidimarri, S. P.; Yoo, J.; Gyenes, B.; Ohmann, A.; Winterhalter, M.; Aksimentiev, A.; Keyser, U. F. Large-Conductance Transmembrane Porin Made from DNA Origami. *ACS Nano* **2016**, *10* (9), 8207–14.
- (31) Burns, J. R.; Stulz, E.; Howorka, S. Self-Assembled DNA Nanopores that Span Lipid Bilayers. *Nano Lett.* **2013**, *13* (6), 2351–6.
- (32) Burns, J. R.; Gopfrich, K.; Wood, J. W.; Thacker, V. V.; Stulz, E.; Keyser, U. F.; Howorka, S. Lipid-Bilayer-Spanning DNA Nanopores with a Bifunctional Porphyrin Anchor. *Angew. Chem., Int. Ed.* **2013**, *52* (46), 12069–72.
- (33) Bell, N. A. W.; Keyser, U. F. Nanopores Formed by DNA Origami: A Review. *FEBS Lett.* **2014**, *588* (19), 3564–3570.
- (34) Gopfrich, K.; Zettl, T.; Meijering, A. E. C.; Hernández-Ainsa, S.; Kocabey, S.; Liedl, T.; Keyser, U. F. DNA-Tile Structures Induce Ionic Currents through Lipid Membranes. *Nano Lett.* **2015**, *15* (5), 3134–3138.
- (35) Wei, R.; Martin, T. G.; Rant, U.; Dietz, H. DNA Origami Gatekeepers for Solid-State Nanopores. *Angew. Chem., Int. Ed.* **2012**, *51* (20), 4864–4867.
- (36) Fennouri, A.; List, J.; Dupasquier, J.; Haeni, L.; Vanni, S.; Rothen-Rutishauser, B.; Mayer, M. Templated Assembly of Pore-Forming Peptides in Lipid Membranes. *CHIMIA International Journal for Chemistry* **2019**, *73* (1), 59–62.
- (37) Henning-Knechtel, A.; Knechtel, J.; Magzoub, M. DNA-Assisted Oligomerization of Pore-Forming Toxin Monomers into Precisely-Controlled Protein Channels. *Nucleic Acids Res.* **2017**, *45* (21), 12057–12068.
- (38) Saint, N.; Marri, L.; Marchini, D.; Molle, G. The Antibacterial Peptide Ceratotoxin A Displays Alamethicin-Like Behavior in Lipid Bilayers. *Peptides* **2003**, *24* (11), 1779–1784.
- (39) Boheim, G. Statistical Analysis of Alamethicin Channels in Black Lipid Membranes. *J. Membr. Biol.* **1974**, *19* (1), 277–303.
- (40) Bessin, Y.; Saint, N.; Marri, L.; Marchini, D.; Molle, G. Antibacterial Activity and Pore-Forming Properties of Ceratotoxins: A Mechanism of Action Based on the Barrel Stave Model. *Biochim. Biophys. Acta, Biomembr.* **2004**, *1667* (2), 148–156.
- (41) Mayer, S. F.; Ducrey, J.; Dupasquier, J.; Haeni, L.; Rothen-Rutishauser, B.; Yang, J.; Fennouri, A.; Mayer, M. Targeting Specific Membranes with an Azide Derivative of the Pore-Forming Peptide Ceratotoxin A. *Biochim. Biophys. Acta, Biomembr.* **2019**, *1861* (10), 183023.
- (42) Zhang, L.; Benz, R.; Hancock, R. E. W. Influence of Proline Residues on the Antibacterial and Synergistic Activities of α -Helical Peptides. *Biochemistry* **1999**, *38* (25), 8102–8111.
- (43) Chen, B.; Le, W.; Wang, Y.; Li, Z.; Wang, D.; Ren, L.; Lin, L.; Cui, S.; Hu, J. J.; Hu, Y.; et al. Targeting Negative Surface Charges of Cancer Cells by Multifunctional Nanopores. *Theranostics* **2016**, *6* (11), 1887.
- (44) Uram, J. D.; Ke, K.; Mayer, M. Noise and Bandwidth of Current Recordings from Submicrometer Pores and Nanopores. *ACS Nano* **2008**, *2* (5), 857–872.
- (45) Mayer, M.; Kriebel, J. K.; Tosteson, M. T.; Whitesides, G. M. Microfabricated Teflon Membranes for Low-Noise Recordings of Ion Channels in Planar Lipid Bilayers. *Biophys. J.* **2003**, *85* (4), 2684–2695.
- (46) Fennouri, A.; Mayer, S. F.; Schroeder, T. B. H.; Mayer, M. Single Channel Planar Lipid Bilayer Recordings of the Melittin Variant MelP5. *Biochim. Biophys. Acta, Biomembr.* **2017**, *1859* (10), 2051–2057.
- (47) Wiedman, G.; Fuselier, T.; He, J.; Searson, P. C.; Hristova, K.; Wimley, W. C. Highly Efficient Macromolecule-Sized Poration of Lipid Bilayers by a Synthetically Evolved Peptide. *J. Am. Chem. Soc.* **2014**, *136* (12), 4724–4731.
- (48) Blondelle, S. E.; Houghten, R. A. Novel Antimicrobial Compounds Identified Using Synthetic Combinatorial Library Technology. *Trends Biotechnol.* **1996**, *14* (2), 60–65.
- (49) Hilpert, K.; Volkmer-Engert, R.; Walter, T.; Hancock, R. E. High-Throughput Generation of Small Antibacterial Peptides with Improved Activity. *Nat. Biotechnol.* **2005**, *23* (8), 1008.
- (50) Garni, M.; Thamboo, S.; Schoenenberger, C.-A.; Palivan, C. G. Biopores/Membrane Proteins in Synthetic Polymer Membranes. *Biochim. Biophys. Acta, Biomembr.* **2017**, *1859* (4), 619–638.
- (51) Zhang, X.; Fu, W.; Palivan, C. G.; Meier, W. Natural Channel Protein Inserts and Functions in a Completely Artificial, Solid-Supported Bilayer Membrane. *Sci. Rep.* **2013**, *3*, 2196.
- (52) Hall, J. E.; Vodyanoy, I.; Balasubramanian, T. M.; Marshall, G. R. Alamethicin. A Rich Model for Channel Behavior. *Biophys. J.* **1984**, *45* (1), 233–247.
- (53) Marchini, D.; Marri, L.; Rosetto, M.; Manetti, A. G.; Dallai, R. Presence of Antibacterial Peptides on the Laid Egg Chorion of the Medfly *Ceratitis capitata*. *Biochem. Biophys. Res. Commun.* **1997**, *240* (3), 657–663.
- (54) Rello, S.; Stockert, J. C.; Moreno, V.; Gámez, A.; Pacheco, M.; Juarranz, A.; Cañete, M.; Villanueva, A. Morphological Criteria to Distinguish Cell Death Induced by Apoptotic and Necrotic Treatments. *Apoptosis* **2005**, *10* (1), 201–208.
- (55) Miller, C. *Ion Channel Reconstitution*; Springer Science & Business Media: New York, 1986.
- (56) Montal, M.; Mueller, P. Formation of Bimolecular Membranes from Lipid Monolayers and a Study of their Electrical Properties. *Proc. Natl. Acad. Sci. U. S. A.* **1972**, *69* (12), 3561–3566.